A computational study of structural and excitonic properties of chlorosomes

Li, X.

CHAPTER 6

Outlook

Thus far, we have considered structural properties of tubular aggregates as simulated by MD at finite temperature, starting from pre-packed (flat and tubular) quasi-2D structures of unit cells that correspond to a *syn-anti* packing model, investigated the excitonic properties of closed and stable (multi)tubes, and eventually gained insights into the microscopic origin of efficient energy transfer in chlorosomes. I hope that both our results and protocols/strategy will help future studies of researchers that focus on chlorosomes or other large tubular molecular aggregates. Of course, to get to this point, other options and properties were considered. In this final chapter, I outline some novel research ideas and initial results that did not make it to the body of my thesis, and that address different aspects of chlorosomes. They deal with the assembly kinetics and mechanical properties of these aggregates, and particularly focus on, and to some extent clarify, the role of the farnesyl tail that are present in all types of BChl pigments.

From Chapter 2, we know that these pigment tails occupy the tiny 2.1 nm space between layers of *syn-anti* stacks and mediate their separation by tight packing. For this reason, we assumed that tails play a vital role in the assembly process and profoundly affect the mechanical properties of chlorosomes. This chapter sheds light on how to validate such an assumption.

6.1. Self-Assembly Kinetics of Chlorosomal Aggregates

One can be easily amazed by chlorosomes found in photosynthetic bacteria. The protein-free strategy that is responsible for the formation of chlorosomes may be utilized for constructing other customized light-harvesting complexes or nanoscale devices. However, attempts to reconstitute tubular aggregates from constituents that were extracted from natural chlorosomes showed a distinct sensitivity to the processing conditions, which illustrates that understanding the precise assembly kinetics of large amounts of BChl molecules into a supramolecular structure is of great significance, albeit that it is fairly limited in practice. Few *in vitro* studies monitored the self-assembly of BChl molecules, or of BChl mimics in different solvent conditions, temperature, or light conditions.[100,180,187,188] In particular, Balaban *et al.*[100] monitored the self-assembly of BChl *c* molecules into large aggregates, which were shown to be the same as those formed *in vivo*, by tuning the concentration of apolar solvent (in their case, hexane) in water. Based on the time variation of the absorption intensity at the Q_y band, they proposed an auto-catalytic self-assembly mechanism of nucleation and growth.

In principle, an *in silico* method like molecular dynamics (MD) can address any assembly kinetics. In practice, however, 'brute force' usage of MD does not work for studying self-assembling of bio-inspired supramolecular systems; for more details, especially for the practical limitations, see a helpful recent review.[51] In particular, the use of all-atom MD for this purpose is restricted by its limited phase-space sampling ability, as discussed in Chapter 1. Considering the actual time and length scales that are needed to address assembly kinetics in a realistic environment, coarse-grained MD may be a solution,[189,190] as it can speed up the phase space sampling ability by several orders of magnitude. However, incorporating the level of detail that is needed to represent the important interactions on the coarser level requires an additional effort.

Coarse-Graining within the Martini Force Field. The Martini force field constitutes one of the most popular coarse-grained methods for bio-molecules.[47] It uses a four-to-one (four heavy atoms to one bead) mapping for obtaining a CG representation; for CG beads, plug-and-play CG force fields (FF) have been developed, in analogy to atomistic FF. Following recently reported Martini representation for similar molecules, chlorophyll (Chl) *a* and *b*,[191,192] we have

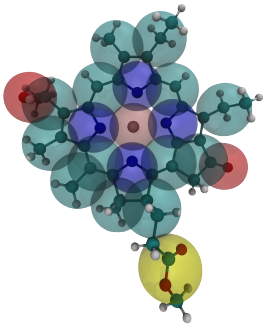

Figure 6.1: Martini CG model for Me-BChl *c* with a methyl ester termination instead of the farnesyl tail in BChl *c*. Large transparent spheres represent the CG interaction sites or beads, and are shown overlapping the atomistic representation. The color blue/green/yellow/red/pink corresponds to the SP3/SC3/NO/SNa or SNd/SQa type of martini particles. Equilibrium bond lengths and angle values are extracted from all-atom MD structures; the strengths of bond and angle constraints are mainly taken from de Jong's work.[191] Following their protocol, the Mg atom is mapped 1:1 to an SQda bead, with charge parameter +1.0; each SP3 bead carries a −0.25 charge, which neutralizes the whole molecule. We also apply certain distance restraints and dihedral angle constraints.

focused on the head part of BChl molecules and developed a Martini representation for Me-BChl *c*, *i.e.* BChl *c* without its (farnesyl) tail and with a methyl ester termination. Figure 6.1 shows the CG description.

We found that the thus constituted CG model reproduces the atomic structure of a single molecule quite well. Nevertheless, the intermolecular structure is more problematic; even the basic packing motifs are lost. As shown in Figure 6.2a, we find H-type aggregates after CGMD simulation, rather than the J-aggregates of all-atom MD (AAMD). Careful analysis shows that the Mg-OH coordination interaction is vital for stabilizing J-type aggregate like chlorosomes. In particular, by increasing the strength of this coordination interaction between SQa-SNd by a 100 times, a chlorosomal *syn-anti* stacking structure is indeed formed, see Figure 6.2b. To recover also other structural features, *e.g.* π-π stacking and hydrogen-bonds, much more effort is needed. We note that excessive tuning of the non-bonded interaction parameters is not recommended in general. One key challenge is the isotropic/spherical shape of the CG potentials with an effective isotropic bead radius of 0.47 nm, which is a general issue in Martini and particularly problematic for reproducing correct π-π stacking interactions that give rise to an average spacing of $\approx$ 0.35 nm. Considering these limitations, it is likely that other types of CG models, for instance based on anisotropic beads such as plate-like particles[193,194] are more promising for BChl-like systems.

6.2. Mechanical Properties of Chlorosomal Tubes

Mechanical properties of natural complexes are of great importance for sustained biological function.[195] In particular, many of these complexes exhibit extraordinary mechanical characteristics. Although tubular aggregates like chlorosomes have been in the focus of researchers for many years, their mechanical properties have neither been well examined experimentally, especially in relation to their molecular building blocks, nor properly examined by theoretical or experimental means. Here, we share results that for the first time consider mechanical properties of chlorosomes, in the form of an outlook that hopefully may convince other researchers in this field that it is an aspect worth studying. In particular, through a systematic study of their mechanical prop-

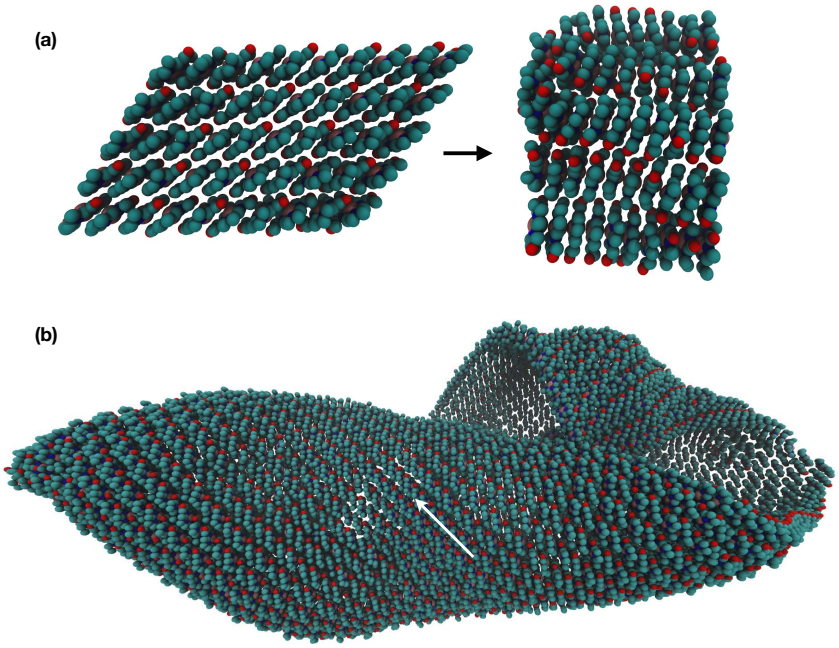

Figure 6.2: Martini CGMD simulation results of structures starting from planar aggregates composed of *syn-anti* dimers. (a) A small aggregate case, snapshots at t = 0 (left) and t = 100 ps (right) (b) A large aggregate case with stronger interaction mimicking the Mg-OH coordination interaction. This snapshot is at t = 200 ps. The white arrow outlines the syn-anti stacking direction.

erties for various chiral angles δ, we may begin to understand the effect of supramolecular chirality on mechanical properties.

6.2.1. Elasticity

When a material undergoes an externally applied stress, it may deform by changing its shapes or size, which is described in terms of strain. In the elastic regime, the material is able to recover its original configuration, shape and size, when the applied stress is removed. The elastic modulus measures the resistance of the material to being deformed elastically; its value can be determined from the slope of the stress-strain curve in the elastic deformation region, see Figure 6.3, which is usually the onset of the curve where the deformation is sufficiently small. Depending on how stress and strain are defined, one can determine different types of elastic moduli, including Young's modulus, shear modulus, bulk modulus, and others. For example, Young's modulus, the most common elastic modulus, quantifies to the elastic property of a material that undergoes tension or compression along a uni-axial direction.

Studying the mechanical properties of chlorosomes experimentally is complicated due to their mesoscopic dimensions and known difficulties in sample preparation. Our progress in constructing realistic atomistic tube structures of chlorosomes, however, provides a unique chance to consider their mechanical properties *in silico*, allowing us to make predictions prior to such experimental studies.

Various approaches can be employed to access the elastic properties of tubular assemblies via MD simulations. One approach uses the relation between equilibrium strain fluctuations and elastic constants to determine the elastic modulus from equilibrium MD simulation trajectories.[196,197] Another approach mimics the protocol in experimental setups, which determines the elastic modulus directly from the measured stress-strain curves. In this approach, one needs to apply an external force to the structure in an equilibrium MD simulation to implement a programmed strain or stress.[198–205] Wells and Aksimentiev[202] illustrated the potential of such a setup for investigating different types of mechanical properties.

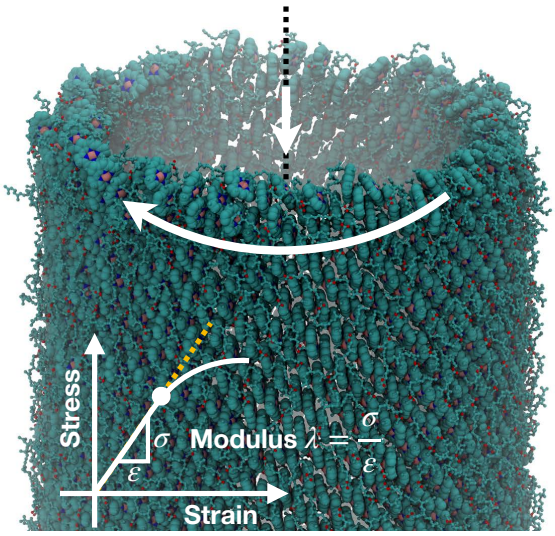

Figure 6.3: Simulation schematics for determining elastic properties based on an all-atom tube structure of chlorosomes. The dashed line represents the tube axis. The elastic modulus is obtained from the relation between strain and stress, as shown in the inset. It is possible to perform different types of deformation to extract different moduli, using a variety of probing methods, for instance by compression or twisting, as labeled by the straight or curved arrows.

6.2.2. Response to Shock Compression

Shock compression plays a role in a material when it is exposed to extreme situations, such as collision, explosion, and explosive welding.[206] In such a case, the material is often stressed far beyond its elastic limit, and shock waves occur.[207] After this shock wave has passed, atomic positions have been changed irreversibly, which means that the material looses the ability to recover its original state.[208] One thus needs to address all detailed microscopic structural deformations in order to understand the consequence of a shock wave on the material.[209]

Non-equilibrium MD simulations have been widely used to investigate the response of materials to shock compression and to examine the detailed shock-wave propagation, for instance, in metals,[206,210–212] polymers,[213–216] small organic molecules,[217] and lipids.[218] It is currently unknown how chlorosomes, as well as other tube molecular aggregates, respond to shock compression, so we employed MD simulations to fill this knowledge gap. As an initial test, we considered the simplest setup for shock compression, and we let the tube structure collide with an immobile wall. Such a method was previously employed to study the impinging process of nanodroplets.[219] In our setup, the tube structure is initially centered in the simulation box *in vacuo*, with its tube axis parallel to the z-direction. An immobile wall is positioned at the bottom of the simulation box, perpendicular to the tube axis. By applying the same, instantaneous velocity v_z to all atoms, in the direction of the wall, the tube structure will eventually collide with the wall and deform, see Figure 6.4 for the consequential compression along the tube axis. This and all other simulations in this section were performed in a NVE ensemble.

Figure 6.4 shows several selected snapshots along an MD trajectory for an initially applied velocity $|v_z| = 500$ m/s, *i.e.* faster than the speed of sound in air. After hitting the wall, the helical tube has to dissipate the additional kinetic energy, and part of the tube close to the wall starts to open outwards (10 ps) into a small deformation zone. Soon after, at 20 ps, modulation of the underlying molecular lattice can be observed along the whole tube. Whether this lattice modulation is the signature of a shock wave, or the onset of structural instability on a larger length scale, we have not considered in detail. However, after 30 ps, the modulations can be seen to decrease, while the size of the outward deformation zone increases. At 130 ps, the deformation

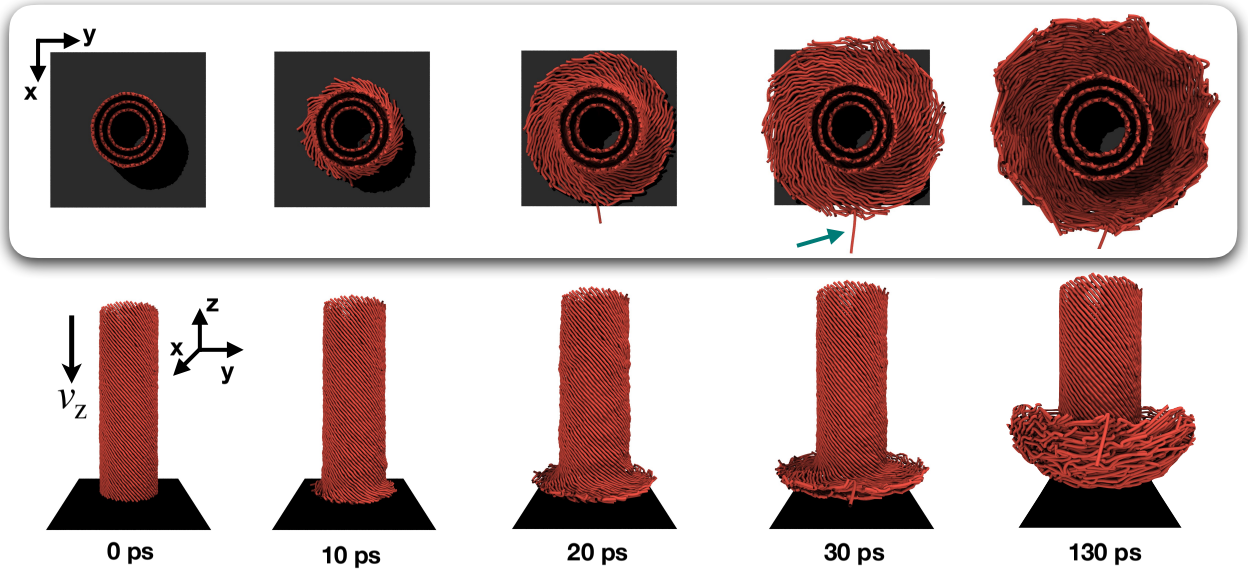

Figure 6.4: Snapshots of an impact compression simulation after an instantaneously applied velocity $|v_z| = 500$ m/s. Snapshots were taken at $t = 0, 10, 20, 30, 130$ ps. The BChl *c* assembly is composed of three concentric tubes. Corresponding orthogonal views along the axis of the tubes are shown on top, since this axis is along the z-direction of the applied velocity. The chosen dimension of the assembly is 60 nm in length, and 20 nm in diameter. Since such a structure contains roughly 1.6 million atoms, we only show helices along the *syn-anti* stacks (in red color) for visual clarity. The immobile wall into which the structure collides is shown in black. As one molecule is detached from its helix, the end of that helix is stretched out in snapshots after 10 ps, as labeled by a green arrow.

zone has even grown larger, and has curled into a half sphere, but the lattice on the remaining part of the tube has completely recovered. At even later stages, the impact of the shock impact fades off, and the evolution of the deformation zone is halted (after 130 ps, not shown). From the orthogonal views in Figure 6.4, it is clear that the helices along the *syn-anti* packing direction are well kept, even thought the contact part is substantially distorted. Simulating impact for an increased $|v_z| = 1000$ m/s shows a similar process, with the curling into a spherical shape further progressing into the upper part of the tube. For a smaller value of $|v_z| = 100$ m/s, we only observe a tiny deformation zone, and almost no change of the overall tube structure.

It is intriguing to see that, when the tube structure has to dissipate much energy for higher impact velocities, it responds by forming a unique outward curling deformation at the contact end of the tube, while keeping a memory of the original state of helices along the *syn-anti* packing direction. It is highly likely that the tails parts of the BChl molecules play an important role in this phenomena, and stabilize the structure under deformation. It would be interesting to see whether the tube can recover from a curling deformation, but we leave such computational experiments for the future. We propose that the tube structure of chlorosomes not only has a functional role in light-harvesting, but that it also provides promising resistance to damage and failure under impact and/or high strain rates,[220] and is likely to have a self-repair ability as observed in microtubule systems.[221]

We realize that, in order to address these mechanical properties of chlorosomes, much more effort is needed. Nevertheless, by providing this general introduction and some of these initial tests, I hope I have aroused the reader's curiosity and drawn more general attention to the unique properties of the *chlorosome*.